# Advanced beamforming and reflection control in intelligent reflecting surfaces with integrated channel estimation

Monga, Sakhshra; Singh, Anmol Rattan; Saluja, Nitin; Prabha, Chander; Malhotra, Shivani; Karim, Asif; Hassan, Md Mehedi

*Published in:*
IET Microwaves, Antennas and Propagation

*DOI:*
10.1049/mia2.12538

Published: 01/12/2024

*Document Version*
E-pub ahead of print

Received: 8 August 2024 | Revised: 19 November 2024 | Accepted: 25 November 2024

IET Microwaves, Antennas & Propagation

DOI: 10.1049/mia2.12538

ORIGINAL RESEARCH

# Advanced beamforming and reflection control in intelligent reflecting surfaces with integrated channel estimation

Sakhshra Monga[1] | Anmol Rattan Singh[1] | Nitin Saluja[1] | Chander Prabha[1] | Shivani Malhotra[1] | Asif Karim[2] | Md. Mehedi Hassan[3]

[1]Chitkara University Institute of Engineering and Technology, Chitkara University, Rajpura, Punjab, India

[2]Faculty of Science and Technology, Charles Darwin University, Casuarina, Northern Territory, Australia

[3]Computer Science and Engineering Discipline, Khulna University, Khulna, Khulna, Bangladesh

**Correspondence**

Md. Mehedi Hassan.
Email: mehedihassan@ieee.org

**Abstract**

Intelligent Reflecting Surfaces (IRS) enhance wireless communication by optimising signal reflection from the base station (BS) towards users. The passive nature of IRS components makes tuning phase shifters difficult and direct channel measurement problematic. This study presents a machine learning framework that directly maximises the beamformers at the BS and the reflective coefficients at the IRS, bypassing conventional methods that estimate channels before optimising system parameters. This is achieved by mapping incoming pilot signals and data, including user positions, with a deep neural network (DNN), guiding an optimal setup. User interactions are captured using a permutation-invariant graph neural network (GNN) architecture. Simulation results show that implicit channel estimation method requires fewer pilots than standard approaches, effectively learns to optimise sum rate or minimum-rate targets, and generalises well. Specifically, the sum rate for GDNNet (GNN + DNN) improves by 12.57% over linear minimum mean square error (LMMSE) and by 12.42% over perfect CSI concerning the number of users, and by 28.57% over LMMSE and by 14.28% over perfect CSI concerning pilot length. Offering a feasible solution with reduced computing complexity for real-world applications, the proposed GNN + DNN method outperforms conventional model-based techniques such as LMMSE and approaches the performance of perfect CSI, demonstrating its high effectiveness in various scenarios.

**KEYWORDS**

5G mobile communication, channel estimation, MIMO communication

## 1 | INTRODUCTION

While deployment of fifth-generation (5G) wireless network is ongoing, researchers are already setting their sights on the next generation, known as sixth-generation (6G) wireless network. The goal for 6G is to surpass capabilities of its predecessor by offering significantly higher throughput, exceptional ultra-low latency, remarkably low power consumption, and reliability [1]. However, achieving these ambitious goals may not be feasible with current technologies alone, such as massive multi-input multi-output (MIMO) and millimetre-wave (mmWave) communications. While these technologies offer improved performance, they often come with increased energy consumption and higher hardware costs. On the other hand, shortcomings in the wireless channel, such as path-loss, shadowing, and small-scale fading, inevitably restrict the performance of wireless communication [2, 3]. While some of these problems can be somewhat resolved using classic wireless communication techniques like power regulation, diversity, adaptive modulation, and dynamic beamforming, they are still very unpredictable and challenging to manage. Conventional methods like minimum mean square error (MMSE) and linear minimum mean square error (LMMSE) offer some mitigation but still face limitations in fully overcoming channel impairments. Intelligent reflecting surfaces (IRS) has recently become a viable technology to address these issues. [4]. By changing the

phase responses of passive materials, IRS has great potential as demonstrated in Figure 1 to steer incident electromagnetic waves into intended directions. Intelligent reflecting surfaces may greatly enhance the channel of communication between the transmitter and receiver by carefully changing these phases, therefore changing the signal propagation environment. Furthermore, IRS's passive character causes it to need less energy to reach the required phase transitions for signal reflection [5].

In a related work, the authors of paper [6] provide a detailed exploration of key signal processing approaches, such as channel estimation, transmission design, and radio localisation for IRS systems. It underscores the critical importance of advanced signal processing techniques in fully harnessing the capabilities of IRS technology. The paper's notable contributions include strategies for overcoming challenges in channel estimation, improving transmission performance, and reducing pilot overhead—factors that are vital for enhancing both spectral and energy efficiency in next-generation wireless communication systems. [7, 8].

Furthermore, it may be easily incorporated into many surfaces, including ceilings and walls, therefore enabling its use in current wireless communication systems. As so, the literature has investigated several uses for IRS. These include improving performance, allowing secured wireless communications, spreading network coverage, increasing wireless spectral efficiency, lowering data transmission power consumption, and so down. This paper addresses the challenge of optimally tuning IRS elements to enhance capacity in a multiuser cellular network. Traditionally, the design process involves initially estimating the channel and subsequently optimising the design parameters [9]. However, this may not be the most effective approach for designing an IRS system for several reasons. Firstly, IRS passive elements lack the capability for active signal transmission and reception, making channel estimation indirect [10]. Secondly, the IRS typically comprises numerous reflective elements, leading to a large number of channel parameters to estimate. Thirdly, conventional channel estimation methods often rely on artificial criteria, such as mean squared error, which may not align with the system's ultimate objective [11, 12]. Finally, optimising phase shifts and beamformers is a challenging high-dimensional non-convex problem with major numerical difficulties even with perfect channel knowledge. This work presents a data-driven method to handle these difficulties [13]. It demonstrates that it is conceivable to immediately learn the mapping from acquired pilot signals to the ideal beamformer settings at the base station (BS) and the final reflecting pattern at the IRS by use of a graph neural network (GNN) architecture modelling the interaction between the IRS and many users. This approach seeks to maximise system-wide goals including the minimum rate among several customers or the aggregate rate. While keeping the IRS reflecting pattern constant, the GNN design combines features that preserve consistent permutation in BS beamformers when the user order is changed. These characteristics, sometimes referred to as permutation equivariant and permutation invariant, allow the network to extend to any conceivable user count [14]. Integrating GNN with deep neural network (DNN) leverages the strengths of both models: the GNN captures user interactions and IRS elements, while the DNN efficiently processes complex data patterns for system optimisation. Numerical results indicate that the proposed approach yields easily interpretable solutions. This study demonstrates that bypassing explicit channel estimation through a machine learning approach can achieve significantly higher transmission rates than traditional methods, particularly with limited pilot lengths.

The two-timescale design provides an alternative for reducing pilot overhead by optimising phase shifts at the IRS based on statistical CSI, which captures long-term stable channel characteristics, while beamforming at the BS is adjusted using instantaneous effective CSI. This approach reduces the dependency of pilot overhead on the number of reflecting elements, making it more efficient for large IRS systems. On the other hand, the proposed GNN+DNN framework focuses on real-time data-driven optimisation, where both the beamforming and phase shifts are directly learnt from pilot signals using GNNs and DNNs. This

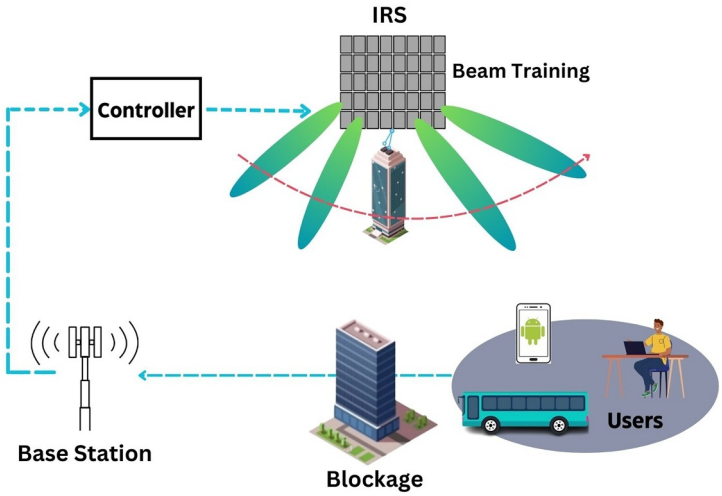


**FIGURE 1** IRS-assisted communication system optimising signal reflection.

approach eliminates the need for explicit channel estimation, allowing for real-time optimisation of configurations, providing greater flexibility and precision in dynamic environments. However, it may result in higher pilot overhead especially with larger IRS setups [15].

The key difference between these methods lies in how they handle pilot overhead and system optimisation. The two-timescale design minimises pilot overhead by using long-term statistical CSI, making it highly scalable for large systems, though it may not adapt as quickly to short-term channel changes. In contrast, the GNN+DNN approach focuses on real-time adaptation, offering immediate optimisation for rapidly changing conditions, but with a potential increase in pilot overhead. Ultimately, the two-timescale design is well-suited for stable large-scale systems, while the GNN + DNN framework excels in dynamic environments that require continuous real-time optimisation. The choice between these approaches depends on the balance between pilot efficiency, real-time adaptability, and the specific needs of the system.

This study utilises time division duplexing (TDD) as the main communication mode, primarily due to its advantages in channel estimation for RIS-assisted systems. With TDD, channel reciprocity is achieved, meaning the uplink and downlink channels have identical characteristics within a coherence interval. This is especially useful in RIS-based setups, which involve numerous reflecting elements that can complicate the estimation process. By leveraging TDD, the system can estimate downlink channels based on uplink pilot signals, reducing pilot overhead and streamlining the channel estimation process.

In the proposed GNN+DNN framework, TDD plays a vital role as it enables the system to optimise both the beamforming at the BS and the phase shifts at the RIS using the same channel data. This approach simplifies the complexity associated with managing separate estimations for uplink and downlink, while also enhancing the system's adaptability in real-time by making more efficient use of the shared channel information.

The machine learning framework is versatile and can be applied to various overall network objectives. Specifically, it demonstrates superior performance in both sum-rate maximisation and minimum-rate maximisation, significantly reducing the length of pilots needed to achieve target performance levels [16]. The interpretability of system-level optimisation solutions is critical for their effective adoption. This work investigates the beamforming and reflecting patterns learnt by the GNN from training data, therefore offering visual proof that the deep learning approach efficiently concentrates electromagnetic waves towards target users. This shows how well the method can locate optimal solutions in the somewhat non-convex optimisation terrain. Combining GNN with DNN improves the learning and generalising capacity of the system and provides a strong and quick answer for IRS-assisted communication systems. In summary, the primary innovations and key findings of this paper include the following.

- The GNN + DNN system maps obtained pilot signals straight to optimal phase shifts at the IRS and beamforming matrices at the BS. Eliminating the explicit channel estimate phase allows this machine learning system to employ pilots more effectively than conventional techniques such LMMSE and perfect CSI.
- At the BS the GNN architecture converts incoming pilot signals into beamformers using reflecting patterns at the IRS. Unlike traditional techniques, its design guarantees permutation invariance for the reflecting pattern and permutation equivariance for user beamformers, therefore enabling the system to adapt to different numbers of users.
- The neural network can integrate various inputs, such as user location data, to enhance system performance. This feature provides a distinct advantage over traditional schemes like LMMSE, which do not typically account for such diverse inputs.
- The GNN + DNN approach generates beamforming patterns that are visualised to show effective learning of the correct beam focussing patterns for both the IRS and BS. This practical efficacy in optimising network performance is not typically achieved by LMMSE and perfect CSI.
- Simulations reveal that the GNN + DNN framework outperforms traditional approaches like LMMSE and closely matches perfect CSI in both sum-rate and minimum-rate maximisation. Additionally, the GNN shows strong generalisation across different signal to noise ratios, demonstrating its robustness and efficiency.

The structure of the paper is as follows: Section 2 reviews the system model. Section 3 details the problem formulation Section 4 focuses on the channel estimation techniques Section 4.4 presents the result and discussion. Finally, Section 5 concludes the paper.

## 2 | SYSTEM MODEL

Consider an IRS-assisted downlink multiuser MISO system in which BS with $M$ antennas serves $K$ users with single-antenna [8]. The communication between BS and users is improved using an IRS with a variety of $E$ passive reflecting devices. The BS operates the IRS via IRS controller, that can adjust phases of the array elements to reflect incident signals in the desired directions, as illustrated in Figure 2.

The uplink channel matrix from IRS to BS is denoted by $\mathbf{O} \in \mathbb{C}^{M\times N}$, uplink channel vector from user $k$ to IRS by $\mathbf{h}_{r,k} \in \mathbb{C}^{N}$, and uplink channel vector from user $k$ to the BS by $\mathbf{h}_{d,k} \in \mathbb{C}^{M}$. With channel reciprocity assumed, the downlink channel matrices correspond to the transposes of these uplink channels. Let $s_k \in \mathbb{C}$ be the symbol intended for user $k$ from the BS. The BS utilises a beamforming vector $\mathbf{w}_k \in \mathbb{C}^{M}$ for transmitting $s_k$, with the beamformers constrained by the power limit $\sum_{k=1}^{K}\|\mathbf{w}_k\|^2 \le P$. The IRS's reflection coefficients are represented as $\boldsymbol{\upsilon} = \left[e^{j\omega_1}, e^{j\omega_2}, \ldots, e^{j\omega_N}\right]^T$, where $\omega_i \in [-\pi, \pi]$

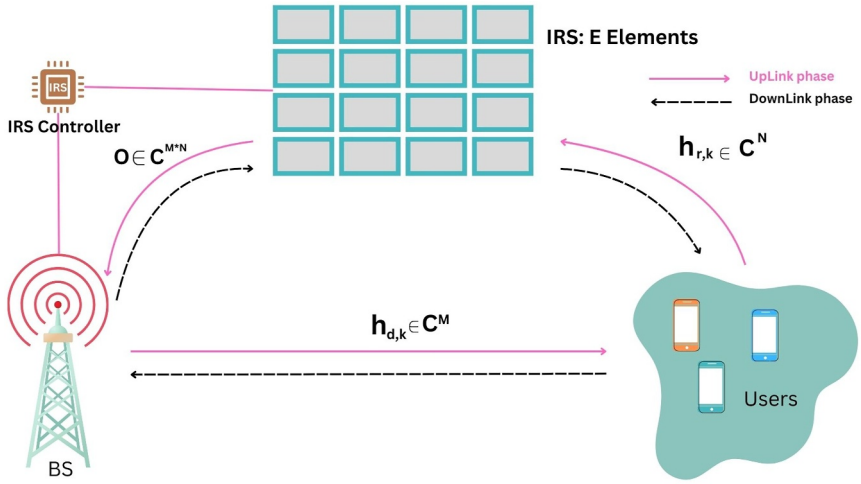


**FIGURE 2** IRS-aided multiuser system.

denotes the phase shift for the $i$th element. The received signal $r_k$ at user $k$ is then expressed as follows:

$$r_k = \sum_{m=1}^{K} \left(\mathbf{h}_{d,k} + \mathbf{O}\,\mathrm{diag}(\boldsymbol{\upsilon})\mathbf{h}_{r,k}\right)^T \mathbf{w}_m s_m + n_k \tag{1}$$

$$r_k = \sum_{m=1}^{K} \left(\mathbf{h}_{d,k} + \mathbf{Q}_k(\boldsymbol{\upsilon})\right)^T \mathbf{w}_m s_m + n_k \tag{2}$$

where $\mathbf{Q}_k = \mathbf{O}\,\mathrm{diag}\left(\mathbf{h}_{r,k}\right)$ represents the cascaded channel, as shown in Table 1, between user $k$ and the BS via reflections at the IRS.

The block-fading model is considered in which channel coefficients vary independently between blocks while staying constant within a coherence block. The achievable rate $A_k$ for user $k$ can be calculated by treating multiuser interference as noise [16].

$$A_k = \log\left(1 + \frac{\left|\left(\mathbf{h}_{d,k} + \mathbf{Q}_k\boldsymbol{\upsilon}\right)^T \mathbf{w}_k\right|^2}{\sum_{i=1,i\neq k}^{K}\left|\left(\mathbf{h}_{d,k} + \mathbf{Q}_k\boldsymbol{\upsilon}\right)^T \mathbf{w}_i\right|^2 + \sigma_0^2}\right) \tag{3}$$

Joint optimisation of the beamforming vectors $\mathbf{w}_k$ at BS and phase shifts $\boldsymbol{\upsilon}$ at IRS maximises a network utility function $U(A_1, A_2, \ldots, A_k)$ depending on the possible rates for all users. Typical user metrics include total rate $\sum_{k=1}^{K} A_k$ and minimum rate $\min_k A_k$.

To optimise BS transmit beamformers and IRS reflection coefficients, knowledge of cascaded channel matrix $\mathbf{Q}_k$ and channel vector $\mathbf{h}_{d,k}$ is essential [17]. This is obtained through the uplink pilot transmission phase where each user $k$ sends a pilot sequence $x_k(\tau)$, reflected by IRS and received at BS, enabling channel estimation via uplink–downlink reciprocity.

$$y_l = \sum_{m=1}^{K} \left(\mathbf{h}_k^d + \mathbf{G}\,\mathrm{diag}(\boldsymbol{\upsilon}(l))\mathbf{h}_k^r\right) x_k(l) + n(l) \tag{4}$$

**TABLE 1** List of symbols and their description of the system model.

| Symbol | Description | Symbol | Description |
|---|---|---|---|
| $M$ | Number of antennas | $K$ | Number of users |
| $E$ | Number of IRS elements | $\mathbf{h}_{d,k}$ | Channel of BS-User |
| $\mathbf{O}$ | Common channel of BS–IRS | $\mathbf{h}_{r,k}$ | Channel of User-IRS |
| $n$ | Additive white Gaussian noise | $l$ | Time slot |
| $U$ | Utility function | $s_k$ | Transmitted pilot signal |
| $\boldsymbol{\vartheta}_t$ | Phase shifting vector | $t$ | Time index |
| $\mathbf{Q}_k$ | Cascaded channel of user-BS | $\mathbf{x}_k$ | Pilot sequence |
| $r_k$ | Received signal at user | $\mathbf{Y}$ | Received signal at BS |
| $L$ | Total number of training slots | $A_k$ | Achievable rate |
| $\boldsymbol{\upsilon}$ | Reflection coefficients | $\mathbf{w}_k$ | Beamforming decoding function |

In this setup, $\mathrm{diag}(\boldsymbol{\upsilon}(\tau))$ is the diagonal matrix containing the IRS phase shifts for time slot $\tau$, and $n(\tau) \sim \mathbb{CN}(0, \sigma^2 I)$ represents additive Gaussian noise [18]. With these $(M+N)K + MN$ unidentified channel coefficients, channel estimation becomes challenging with short pilot lengths.

## 3 | PROBLEM FORMULATION

The basic notion of this article is to optimise the rates $R_k$ directly by efficiently employing the pilot phase [9]. Rather than guessing all channel coefficients, the technique includes mapping received pilots to an optimum transmission strategy for rate maximisation, hence avoiding the channel estimation procedure [19].

In order to do this, the received pilots, $\mathbf{Y}$, are used to design optimal beamforming vectors $\mathbf{w}_k$ and reflection phase

shift $\boldsymbol{\upsilon}$. The pilots received over $L$ symbol durations are denoted by $\mathbf{Y} = [\mathbf{y}_1, \mathbf{y}_2, \ldots, \mathbf{y}_L] \in \mathbb{C}^{M \times L}$. Its purpose is to employ the matrix $\mathbf{Y}$ to solve the following optimisation problem:

$$\max_{\mathbf{W}, \boldsymbol{\upsilon}} \mathbb{E}\left[\sum_k R_k(\boldsymbol{\upsilon}, \mathbf{W})\right] \tag{5}$$

$$\text{subject to} \quad \sum_k \|\mathbf{w}_k\|^2 \leq P, \tag{6}$$

$$|v_i| = 1, \quad i = 1, 2, \ldots, N$$

While $f$ and $g$ map the received pilots to the beamforming matrix $\mathbf{W}$ and phase shifts $\boldsymbol{\upsilon}$, $\mathbf{W} = (\mathbf{w}_1, \mathbf{w}_2, \ldots, \mathbf{w}_k)$ represents the beamforming matrix at the BS here. Across all channels, the anticipation permeates the fast-fading components. However, solving this problem involves non-convex conditions and a non-convex objective function, creating computational difficulties due to its variational optimisation nature. Leveraging the universal approximation capacity of neural networks [20], the mapping functions $f$ and $g$ are suggested to be learnt using deep learning to handle this complexity. Before exploring this method, a baseline solution for this problem is described using the traditional approach of uplink channel estimation, including sum-rate maximisation.

## 4 | TRANSMISSION OF PILOTS AND CHANNEL ESTIMATION TECHNIQUES

The traditional approach for addressing issue (6) comprising an uplink channel estimation phase followed by a downlink utility maximising phase, is described in this part. The downlink utility maximising issue is widely investigated after the channels are approximated [21]. Algorithims for downlink sum-rate maximisation, for instance, are covered in the paper [22], and minimum rate maximisation is investigated in the paper [23]. Here the uplink pilot transmission and channel estimate process takes front stage.

### 4.1 | Pilot transmission in uplink

The pilot transmission strategy from [24] divides the total training slots $L$ into $\tau$ sub-frames, each containing $C_0 = K$ symbols (i.e., $C = \tau C_0$). During these sub-frames, users sequentially transmit their pilot sequences $\mathbf{x}_k^H$ to the BS, repeating this process over the $\tau$ sub-frames [25]. The pilot sequences are orthogonal, allowing decorrelation at the BS, with $\mathbf{x}_k^H \mathbf{x}_{k'} = 0$ for $k \neq k'$ and $\mathbf{x}_k^H \mathbf{x}_k = C_0 P_u$. The IRS maintains its phase shift constant within a sub-frame but varies them across sub-frames to enable the measurement of user-to-IRS and IRS-to-base station channels.

$$\overline{\mathbf{Y}}_t = \sum_{k=1}^{K} \left(\mathbf{h}_{d,k} + \mathbf{O}\,\mathrm{diag}(\overline{\boldsymbol{\upsilon}}(t))\mathbf{x}_k^H\right) + \overline{\mathbf{N}}(t) \tag{7}$$

Base Station decorrelates received pilots in each sub-frame by aligning them with pilot sequence of each user. Here $\overline{\mathbf{Y}}(t) = \left[\mathbf{y}_{(t-1)C_0+1}, \ldots, \mathbf{y}_{tC_0}\right]$ represent received pilots in sub-frame $t$. Let $\overline{\boldsymbol{\upsilon}}(t)$ denote phase shifts at IRS in sub-frame $t$. The received pilots $\overline{\mathbf{Y}}(t)$ can then be described as follows:

$$\overline{\mathbf{y}}_k(t) = \frac{1}{L_0}\overline{\mathbf{Y}}(t)\mathbf{x}_k = \mathbf{h}_{d,k} + \mathbf{Q}_k\overline{\boldsymbol{\upsilon}}(t) + \overline{\mathbf{n}}(t) \tag{8}$$

$$\triangleq \mathbf{F}_k\mathbf{q}(t) + \overline{\mathbf{n}}(t) \tag{9}$$

In this case, a noise matrix with each column independently distributed as $\mathbb{CN}(0, \sigma^2 I)$ is represented as $\overline{\mathbf{N}}(t)$. Due to orthogonality of pilot sequences, contribution from user $k$ in the $t$-th sub-frame, denoted as $\overline{\mathbf{y}}_k(t) \in \mathbb{C}^M$, can be extracted, as described in the paper [26].

Here, $\overline{\mathbf{n}}(t) = \frac{1}{L_0}\overline{\mathbf{N}}(t)\mathbf{x}_k$, and combined channel matrix is described as $\mathbf{F}_k = \left(\mathbf{h}_{d,k}, \mathbf{A}_k\right)$, with the combined phase shifts denoted as $\mathbf{q}(t) = \left[1, \overline{\boldsymbol{\upsilon}}(t)^T\right]^T$. With $\tau$ sub-frames in total, the matrix of received pilots across these sub-frames is denoted as $\tilde{\mathbf{Y}}_k = \left(\overline{\mathbf{y}}_k(1), \overline{\mathbf{y}}_k(2), \ldots, \overline{\mathbf{y}}_k(\tau)\right)$.

$$\tilde{\mathbf{Y}}_k = \mathbf{F}_k\mathbf{J} + \tilde{\mathbf{N}} \tag{10}$$

Also, combined matrix $\mathbf{F}_k$ where $k = 1, \ldots, K$ is sought to be estimated via a channel estimation problem. At least $\tau = N + 1$ sub-frames are needed to guarantee that the matrix $\mathbf{J}$ has full rank, hence enabling effective recovery of $\mathbf{F}_k$. This amounts to a total of $(N+1)K$ pilot signals. A common choice for $\tau = N + 1$ is a DFT matrix, as advised in the paper [16]. For situations when $\tau \neq N + 1$, $\mathbf{J}$ does not have a square form. Starting with a $b \times b$ DFT matrix $\mathbf{Q}'$ having $b = \max(\tau, N + 1)$, then trim $\mathbf{J}'$ to either the first $\tau$ columns or the first $N + 1$ rows. Construct the vectors $\overline{\boldsymbol{\upsilon}}(t)$ randomly, with the phase of $\overline{\boldsymbol{\upsilon}}(t)_i$ selected from a uniform distribution over $[-\pi, \pi)$. This paper uses the random construction method for $\tau < N + 1$ and the truncated DFT matrix method otherwise, as these have been found to work well empirically.

### 4.2 | Linear minimum mean square error based channel estimation technique

To approximate the channel matrix $\mathbf{F}_k$ from equation (10), the minimum mean-squared error (MMSE) estimator is utilised [27]. This estimator is derived by solving the following optimisation problem:

$$\min_{f(\cdot)} \mathbb{E}\left[\left\|f\left(\tilde{\mathbf{Y}}_k\right) - \mathbf{F}_k\right\|_F^2\right] \tag{11}$$

The optimal resolution for the problem presented in equation (11) is provided by reference.

$$f\left(\tilde{\mathbf{Y}}_k\right) = \mathbb{E}\left[\mathbf{F}_k|\tilde{\mathbf{Y}}_k\right] \tag{12}$$

The optimal solution, as noted, requires significant computational resources due to the necessity of high-dimensional integration. To reduce complexity, the estimator $h$ can be restricted to a linear form, leading to the LMMSE method. Consequently, the solution to equation (11) can be described in a closed form, as shown in the paper [28].

$$\hat{\mathbf{F}}_k = \left(\tilde{\mathbf{Y}}_k - \mathbb{E}\left[\tilde{\mathbf{Y}}_k\right]\right)\mathbb{E}\left[\tilde{\mathbf{Y}}_k^H\tilde{\mathbf{Y}}_k\right]^{-1}\mathbb{E}\left[\tilde{\mathbf{Y}}_k^H\mathbf{F}_k\right] + \mathbb{E}[\mathbf{F}_k] \tag{13}$$

The estimates of $\mathbf{h}_{d,k}$ and $\mathbf{Q}_k$ can be directly derived from $\hat{\mathbf{F}}_k$. It is important to acknowledge that a linear constraint on function $h$ may lead to a suboptimal solution for equation (11); this approach achieves optimality only when the unknown $\mathbf{F}_k$ follows a Gaussian distribution.

## 4.3 | Proposed channel estimation technique

The traditional channel estimation method focuses on estimating $\mathbf{F}_k$ as shown in Table 2 using received pilots $\hat{\mathbf{F}}_k$ based on mean squared error. Furthermore, the goal is to maximise network utility. This paper proposes bypassing explicit channel estimation, directly solving the problem by employing a neural network to model the function $g(\cdot)$. Neural network is trained to map received pilot signals to phase shifts and beamformers, optimising network utilisation. In multiuser networks, a GNN approach represents beamformers as shown in Figure 3 and IRS phase shifts with $K+1$ nodes, refining vectors $\mathbf{z}_k$ for beamforming and reflection. GNNs efficiently handle user-IRS interactions, maintain permutation invariance and equivariance, and adapt to varying user numbers. The proposed GNN + DNN scheme enhances this approach, optimising network utility with low complexity. The corresponding neural network architecture is outlined in Figure 3.

### 4.3.1 | Phase shift optimisation

The phase shift optimisation challenge within communication systems focuses on maximising the overall sum rate by fine-tuning the phase shifts of IRS elements. The core objective is to optimise the sum rate across all users, mathematically expressed as follows:

$$\underset{\mathbf{\Theta}^{\chi},\eta}{\text{maximize}} \sum_{k\in\kappa}\log_2\left(1+\eta_k\right) \tag{14}$$

where $\mathbf{\Theta}^{\chi}$ denotes the phase shift matrix for IRS elements, and $\eta_k$ represents the signal-to-interference-plus-noise ratio (SINR) for $k$-th user. Here, $K$ is the set of all users. The SINR for each user must satisfy the condition

$$\eta_k \le \frac{\left|\sum_{l=1}^{L}\mathbf{h}_{kl}^H\mathbf{\Phi}_l^{\chi}\mathbf{G}_l\mathbf{w}_k\right|^2}{\sum_{i\in\kappa,i\neq k}\left|\sum_{l=1}^{L}\mathbf{h}_{kl}^H\mathbf{\Phi}_l^{\chi}\mathbf{G}_l\mathbf{w}_i\right|^2+\sigma^2} \tag{15}$$

**TABLE 2** List of symbols and their description of channel estimation techniques.

| | | | |
|---|---|---|---|
| $\boldsymbol{\tau}$ | Number of sub-frames | $P$ | Transmitted power |
| $C_0$ | Number of symbols in each sub-frame | $\mathbb{E}(\cdot)$ | Expectation operator |
| $\mathbf{F}_k$ | Combined channel matrix for user | $\mathbf{q}(t)$ | Combined phase shift vector in sub-frame $t$ |
| $\mathbf{J}$ | Matrix related to IRS phase shifts, used for channel estimation | $\mathbf{J}'$ | DFT matrix |
| $\mathbb{C}^{N\times M}$ | Complex matrices with $N$ rows and $M$ columns | $\mathbb{C}^{M\times 1}$ | Complex column vector with $M$ entries |
| $b$ | Dimension parameter for DFT matrix construction | $\mathbf{F}_k$ | Combined channel matrix for user |
| $\mathbb{C}^{N\times 1}$ | Complex column vector with $N$ entries | $\mathbb{C}^{N\times N}$ | Complex square matrix with $N\times N$ entries |
| $\mathbb{C}^{M\times M}$ | Complex square matrix with $M\times M$ entries | $f(\cdot)$ | Function representing the MMSE estimator |
| $\mathbf{\Theta}^{\chi}$ | Phase shift matrix for the IRS elements | $\Phi_l$ | Diagonal matrix of phase shifts for the $l$-th IRS element |
| $\eta$ | Signal-to-interference-plus-noise ratio | $\mathbf{G}$ | Channel gain matrix from IRS to the BS |
| $\boldsymbol{\sigma}^2$ | Noise power | $s^{\chi}$ | Complex exponential of the phase shift for IRS element |
| $\boldsymbol{t}_k$ | Vector capturing the combined channel gain and phase shift effects | $\alpha_k$ | Slack variable introduced to simplify optimisation constraints |
| $\boldsymbol{\gamma}_k$ | Slack variable used in beamforming optimisation | $\zeta_k$ | SINR-related variable in beamforming optimisation |
| $z_0^{k^2}$ | Initial representation vector for user node | $D$ | GNN architecture layers |

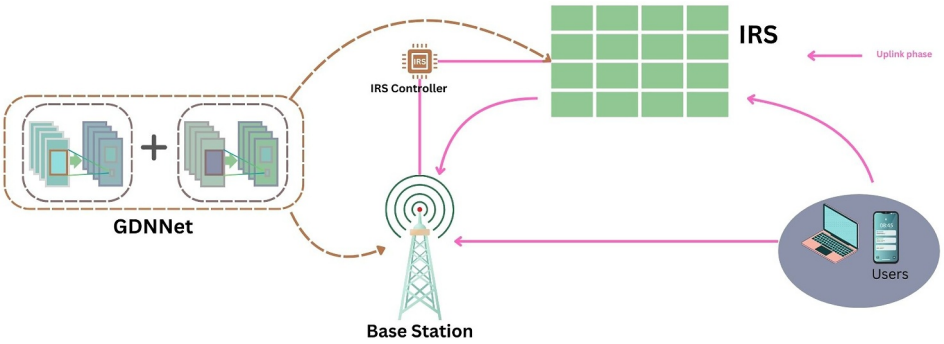


**FIGURE 3** GDNNet-powered intelligent reflecting surfaces (IRS) system for uplink communication optimisation.

with $\mathbf{h}_{kl}$ being the channel coefficient between the $l$-th IRS element and the $k$-th user, $\mathbf{\Phi}_l^{\chi}$ the diagonal matrix of phase shifts for the $l$-th element, $\mathbf{G}_l$ the channel gain matrix from the $l$-th IRS element to the BS, $\mathbf{w}_k$ and $\mathbf{w}_i$ the beamforming vectors for users $k$ and $i$ respectively, and $\sigma^2$ representing the noise power [29]. The phase shifts, denoted as $\theta_{lm}^k$, are constrained within $[0, 2\pi]$ for each element, where $L$ denotes the set of IRS elements, and $M$ is the number of elements per IRS.

To tackle the problem's non-convex nature, the phase shifts are represented using $s_{\ln}^{\chi} = e^{i\theta_{l1}^{\chi}}, \ldots, e^{i\theta_{lN}^{\chi}}$, which captures the complex exponential of each phase shift. The SINR constraint is thus reformulated using the following vectors

$$\mathbf{t}_{kil} = \left[\operatorname{diag}\left(\mathbf{h}_{kl}^H \operatorname{diag}\left(\beta_l^x\right)\mathbf{G}_l, \mathbf{w}_l\right)\right]$$

yielding the following equation:

$$\eta_k \leq \frac{|\mathbf{t}_{kk}^H \mathbf{s}^{\chi}|^2}{\sum_{i\in\kappa, i\neq k}|\mathbf{t}_{ki}^H \mathbf{s}^{\chi}|^2 + \sigma^2} \tag{16}$$

A penalty method is employed to relax the unit modulus constraint, resulting in an adjusted objective function that includes a penalty term,

$$C\sum_{k=1}^{K}\sum_{l=1}^{L}\sum_{m=1}^{M}\left(\left|\mathbf{s}_{lm}^{\chi}\right|^2 - 1\right)$$

where $C$ is a large positive constant.

The problem is further simplified by introducing a slack variable $\alpha_k$, decomposing the constraints into $\left|\mathbf{t}_{kk}^H \mathbf{s}^{\chi}\right|^2 \geq \alpha_k \eta_k$.

$$\sum_{i\in\kappa, i\neq k}\left|\mathbf{t}_{ki}^H \mathbf{s}^{\chi}\right|^2 + \sigma^2 \geq \alpha_k \tag{17}$$

The non-convex term $|\mathbf{t}_{kk}^H \mathbf{s}^{\chi}|^2$ is approximated using a Taylor series expansion around the current solution, leading to a linear expression as follows:

$$\begin{aligned} &-2\Re\left(\mathbf{t}_{kk}^H (\mathbf{s}^{\chi})^n\right)^H \mathbf{t}_{kk}^H (\mathbf{s}^{\chi} - (\mathbf{s}^{\chi})^n) - \left(\mathbf{t}_{kk}^H (\mathbf{s}^{\chi})^n\right)^2 \\ &+\frac{1}{4}\left[\left(\alpha_k + \eta_k^n\right)^2 - 2\left(\alpha_k^n - \eta_k^n\right)\left(\alpha_k - \eta_k\right)\right. \\ &\left.+\left(\alpha_k^n - \eta_k^n\right)^2\right] \end{aligned} \tag{18}$$

This approach results in a convex optimisation problem that integrates the revised objective function and constraints. The problem is solved iteratively, updating the variables $(\mathbf{s}^{\chi})^{n+1}, (\alpha_k)^{n+1}, (\eta_k)^{n+1}$. This iterative procedure, as detailed in Algorithm 1, ensures the solution converges to a locally optimal point, thus maximising the sum rate through optimal phase shift adjustments.

### 4.3.2 | Beamforming optimisation

Given parameters $\mathbf{\Theta}_x$ and $\boldsymbol{\beta}_x$, optimisation problem (4) can be simplified to maximise the sum of logarithms of $1 + \zeta_k$ for all users $k \in K$ with specific constraints [30]. The objective is to:

$$\underset{\boldsymbol{\omega}, \zeta}{\text{maximize}} \sum_{k\in K}\log_2(1 + \zeta_k) \tag{19}$$

subject to:

$$\zeta_k \leq \frac{\left|\tilde{\mathbf{g}}_k^H \mathbf{w}_k\right|^2}{\sum_{i\in\kappa, i\neq k}\left|\tilde{\mathbf{g}}_k^H \mathbf{w}_i\right|^2 + \sigma^2}, \forall k \in K \tag{20}$$

$$\mathbf{W}^H\mathbf{W} \leq P_{\max} \tag{21}$$

where $\tilde{\mathbf{g}}_k$ is a function of the channel matrices and IRS configuration. To handle these constraints, a slack variable $\gamma_k$ is introduced, transforming the problem into the following equation:

$$\left|\tilde{\mathbf{g}}_k^H \mathbf{w}_k\right|^2 \geq \gamma_k \zeta_k \tag{22}$$

$$\sum_{i\in K, i\neq k} \left|\tilde{\mathbf{g}}_k^H \mathbf{w}_i\right|^2 + \sigma^2 \leq \gamma_k \tag{23}$$

Applying an arbitrary rotation to $\mathbf{w}_k$ renders $\tilde{\mathbf{g}}_k^H$ as a real number, simplifying the constraint to the following equation:

$$\Re\{\tilde{\mathbf{g}}_k^H \mathbf{w}_k\} \geq \sqrt{\gamma_k \zeta_k} \tag{24}$$

Using a first-order Taylor approximation, the concave function $\sqrt{\gamma_k \zeta_k}$ around $\gamma_k^n$ is locally approximated as follows:

$$\Re\{\tilde{\mathbf{g}}_k^H \mathbf{w}_k\} \geq \sqrt{\gamma_k^n \zeta_k^n} + \frac{1}{2}\left(\sqrt{\frac{\gamma_k^n}{\zeta_k^n}}(\zeta_k - \zeta_k^n) + \sqrt{\frac{\zeta_k^n}{\gamma_k^n}}(\gamma_k - \gamma_k^n)\right) \tag{25}$$

Thus, the non-convex problem is reformulated as follows:

$$\underset{\boldsymbol{\omega}, \zeta}{\text{maximize}} \sum_{k\in K} \log_2(1+\zeta_k) \tag{26}$$

$$\mathbf{W}^H \mathbf{W} \leq P_{\max} \tag{27}$$

$$\gamma_k \geq 0, \forall k \in K \tag{28}$$

$$\sum_{i\in K, i\neq k} \left|\tilde{\mathbf{g}}_k^H \mathbf{w}_i\right|^2 + \sigma^2 \leq \gamma_k \tag{29}$$

$$\Re\{\tilde{\mathbf{g}}_k^H \mathbf{w}_k\} \geq \sqrt{\gamma_k \zeta_k} \tag{30}$$

This combined algorithm integrates the phase shifting, and beamforming optimisation steps into a single iterative process, using the successive convex approximation technique for each step and updating the parameters iteratively until convergence as shown in Algorithm 1.

**Algorithm 1. Combined algorithm: integrated DNN + GNN hybrid optimisation for phase shifting and beamforming**

**Require:** Initialisation.
1: Initialise.
  Beamforming matrix $\mathbf{W}^0$
  Phase shift vector $\boldsymbol{\phi}^0$
  Amplitude $\boldsymbol{\beta}^0$
  Set iteration index $n = 0$
2: **Repeat**
3: Phase Shift Optimisation:
  Given $\mathbf{W}^{n-1}$, $\boldsymbol{\beta}^{n-1}$, apply the SCA technique to solve the phase shift optimisation problem.
  Denote the solution as $\boldsymbol{\phi}^n$.
4: Beamforming Optimisation:
  Given $\boldsymbol{\phi}^n$, $\boldsymbol{\beta}^n$, apply the SCA technique to solve the beamforming optimisation problem.
  Denote the solution as $\mathbf{W}^n$.
5: Update:
  $n := n + 1$
6: Convergence Check:
  Assess the fractional increment in the objective function. If it remains below a specified threshold $\epsilon > 0$, stop the iteration.
7: **until** The fractional increment in the objective function remains below a specified threshold $\epsilon > 0$.
8: **Return:**
  Optimised phase shift vector $\boldsymbol{\phi}^* = \boldsymbol{\phi}^n$.
  Optimised beamforming matrix $\mathbf{W}^* = \mathbf{W}^n$.

### 4.3.3 | Proposed GDNNet (GNN+DNN neural network) based channel estimation

Architecture of GNN

An initial layer, followed by $D$ layers, which include multiple aggregation and combination layers, and finally, a last normalising layer define the GNN architecture. Beginning with the first representation vector $\mathbf{z}_0^k$ generated from user node input characteristics, it is updated through the $D$ layers to produce $\mathbf{z}_d^k$ for $d = 1, \ldots, D$. Following this is a linear layer, normalised and used to create $\mathbf{W}$, the beamformer, and $\boldsymbol{\upsilon}$, the phase shifts matrices [31]. It outputs $\mathbf{z}_{D+1}^k$. Figure 3 shows the architecture.

1) Initialisation layer:

In this layer, the input features are accepted from the user nodes, thereby constructing the initial representation vector $\mathbf{z}_0^k$ for $k = 1, \ldots, K$. It then processes these via the first neural network layer to create $\mathbf{z}_1^k$ for $k = 0, 1, \ldots, K$, which is utilised in the succeeding layers. Notably, the IRS node, indexed as $k = 0$, lacks input capabilities as only the users send pilots. The user terminal's input features are the vectorised received signals, specifically the pilot signals, represented as $\tilde{\mathbf{Y}}_k$, with distinct real and imaginary components.

$$\mathbf{z}_k^0 = \left(\text{vec}\left(\Re\left\{\tilde{\mathbf{Y}}_k\right\}\right)^T, \text{vec}\left(\Im\left\{\tilde{\mathbf{Y}}_k\right\}\right)^T\right)^T \tag{31}$$

As previously stated, the neural network can easily integrate additional relevant information about each user into the initial input feature vector $\mathbf{z}_0^k$. For instance, if user locations are known, they can be included in the input feature vector $\mathbf{z}_0^k$.

$$\mathbf{z}_k^0 = \left(\mathrm{vec}\left(\Re\left\{\tilde{\mathbf{Y}}_k\right\}\right)^T, \mathrm{vec}\left(\Im\left\{\tilde{\mathbf{Y}}_k\right\}\right)^T, \mathbf{l}_k^T\right)^T \tag{32}$$

where $\mathbf{l}_k$ represents a three-dimensional vector indicating the coordinates of user $k$'s position.

Using the initial input feature vector $\mathbf{z}_0^k$, a layer consisting of entirely connected neuron networks, represented as $f_o^w(\cdot)$, generates $\mathbf{z}_1^k$ for the user nodes [31].

$$\mathbf{z}_k^1 = f_w^0\left(\mathbf{z}_k^0\right), \quad k = 1, 2, \ldots, K \tag{33}$$

For the IRS node, inputs are gathered from all user nodes and initially processed using a permutation-invariant function $\psi_o(\cdot)$, followed by a fully connected neural network $f_o^v(\cdot)$.

$$\mathbf{z}_0^1 = f_v^0\left(\psi_0\left(\mathbf{z}_1^0, \ldots, \mathbf{z}_K^0\right)\right) \tag{34}$$

In the implementation, $\psi_o$ is selected as the element-wise mean function, meaning that each element's average is calculated.

$$\left(\psi_0\left(\mathbf{z}_1^0, \ldots, \mathbf{z}_K^0\right)\right)_i = \frac{1}{K}\sum_{k=1}^{K}\left[\mathbf{z}_k^0\right]_i \tag{35}$$

This choice is logical since all pilots are uniformly reflected through the IRS, providing equal information about it. The representation vectors $\left(\mathbf{z}_0^1, \mathbf{z}_1^1, \ldots, \mathbf{z}_K^1\right)$ now include features for the IRS and user channels. These are processed through the $D$ layers of the GNN, yielding $\boldsymbol{\upsilon}$ from $\mathbf{z}_0^D$, the IRS reflective coefficients, and $\mathbf{w}_k$ from $\mathbf{z}_k^D$, the user beamformers.

2) Updating layers: In the $d$-th layer, the update of the representation vector $\mathbf{z}_k$ entails mixing its prior representation with the aggregated representations from surrounding nodes, provided as follows:

$$\mathbf{z}_k^d = f_{\mathrm{comb}}^d\left(\mathbf{z}_k^{d-1}, f_{\mathrm{aggr}}^d\left(\left\{\mathbf{z}_j^{d-1}\right\}_{j\in\mathbb{N}(k)}\right)\right) \tag{36}$$

A crucial aspect in designing the GNN is selecting appropriate aggregation function $f_{\mathrm{aggr}}^d(\cdot)$ and combining function $f_{\mathrm{comb}}^d(\cdot)$, ensuring scalability and good generalisation. An efficient implementation of $f_{\mathrm{aggr}}^d(\cdot)$ is as follows:

$$f_{\mathrm{aggr}}^d\left(\left\{\mathbf{z}_j^{d-1}\right\}_{j\in\mathbb{N}(k)}\right) = \psi\left(\left\{f_{\mathrm{nn}}^d\left(\mathbf{z}_j^{d-1}\right)\right\}_{j\in\mathbb{N}(k)}\right) \tag{37}$$

The function $\psi(\cdot)$ is invariant to the permutation of inputs, such as element-wise max-pooling or mean pooling, while $f_{\mathrm{nn}}^d(\cdot)$ is implemented as a fully connected neural network. Additionally, the combining function $f_{\mathrm{comb}}^d(\cdot)$ can also utilise a fully connected neural network, particularly for handling complex problems related to optimisation.

3) Normalisation layer:

Following the $D$ update layers, the GNN generates representation vectors $\mathbf{z}_k^D$ for $k = 0, 1, 2, \ldots, K$ for $\boldsymbol{\upsilon} \in \mathbb{C}^N$, which are then passed through a normalisation layer. This stage provides the beamforming matrix $\mathbf{W} \in \mathbb{C}^{M\times N}$ and $\boldsymbol{\upsilon} \in \mathbb{C}^N$, the reflective coefficients, ensuring that the unit modulus restrictions and total power restrictions are properly maintained on $\boldsymbol{\upsilon}$ and $\mathbf{W}$, respectively.

To achieve this, $\mathbf{z}_0^D$ is initially put into a linear layer $f_\upsilon^{D+1}(\cdot)$, consisting of $2N$ fully connected units.

This architecture enables the GNN to adapt to an IRS network with any number of users. The learnt integration and aggregation functions do not depend on the user count. Consequently, altering the user count is simply a matter of adjusting the graph's number of nodes; the existing algorithms for combining and aggregating can still be utilised without the necessity of re-training the artificial neural network.

$$\mathbf{z}_0^{D+1} = f_\nu^{D+1}\left(\mathbf{z}_0^D\right) \in \mathbb{R}^{2N} \tag{38}$$

### 4.3.4 | DNN-driven intelligent reflecting surfaces architecture

To achieve satisfactory power gain, IRS typically deploys dozens or hundreds of reflecting elements, which results in high complexity when adjusting phase of each element individually using conventional algorithms. To mitigate this issue, a DNN is developed to optimise $\boldsymbol{\theta}$.

DNN Architecture

Figure 3 depicts the entire framework of the proposed DNN. The initial layer inputs combined information from IRS-user and BS–IRS channels as training data. A flatten layer then transforms this high-dimensional channel data into a one-dimensional format for processing by subsequent dense layers. Our design employs five dense layers with neuron counts of $16M$, $8M$, $4M$, $2M$, and $M$, respectively. This DNN design cannot directly handle IRS phase shifts due to several preliminary issues. To address gradient vanishing and explosion and to accelerate convergence, a batch-normalisation (BN) layer is added before each dense layer to standardise data mean and variance. Additionally, the activation function $f(x) = \max(x, 0)$ is used to prevent gradient issues and achieve non-linearity. Given that the IRS only adjusts the phase of the signal without altering amplitude reflection coefficients, the reflection matrix elements $\boldsymbol{\Theta}$ are complex values with constant modulus constraints. These constraints cannot be processed by

a standard learning framework. Consequently, a custom Lambda layer is incorporated after the final dense layer to convert the real-valued input vector $\boldsymbol{\theta}_{\text{in}}$ into a constant-modulus complex-valued output vector $\boldsymbol{\theta}_{\text{out}}$.

$$\boldsymbol{\theta}_{\text{out}} = \cos(\boldsymbol{\theta}_{\text{in}}) + \text{j}\sin(\boldsymbol{\theta}_{\text{in}}) \tag{39}$$

Based on the enhanced mechanisms discussed, the DNN is ultimately utilised to optimise the IRS. The detailed parameters of the proposed DNN within the IRS-assisted mmWave MIMO system include $N_{\text{t}} = 64$, $N_{\text{r}} = 16$, and $M = 256$.

The IRS functions as an "intelligent bridge" facilitating communication between the BS and the user, with the optimisation of the reflection matrix $\boldsymbol{\Theta}$ being closely related to the BS–IRS channel $\mathbf{G}$ and the IRS-user channel $\mathbf{H}_r$. Accordingly, the DNN employs combined channel information $\mathbf{H}_c = \mathbf{H}_r\mathbf{G}$ as input data for network training. Since the DNN is real-valued, $\mathbf{H}_c \in \mathbb{C}^{N_r \times N_t}$ is expanded into three parts: the real part, imaginary part, and absolute value of the combined channel matrix [32]. The absolute value, an important parameter characterising channel attenuation, is included to enhance the network's ability to distinguish different channel conditions. To ensure the trained network adapts well to complex real-world environments, a dataset of 640,000 combined channels is generated.

## 4.4 | Result and discussion

This section delivers a detailed evaluation of the GNN + DNN framework's effectiveness in IRS-assisted systems. Through simulations and comparisons, this section reveals how the GDNNet model significantly boosts sum-rate, reduces pilot requirements, and optimises beamforming and phase shifts across diverse settings. The analysis highlights the model's scalability and consistent outperformance of traditional methods like LMMSE and perfect CSI, affirming its potential for complex multiuser scenarios in 5G and 6G environments.

### 4.4.1 | Simulation setup

In an IRS-assisted multi-user MIMO communication system for an indoor scenario as shown in Figure 4. The setup includes a BS with 4 antennas and an IRS comprising 100 passive elements. Two users are uniformly distributed within a circular area centred at coordinates (14 m and 3 m) with a radius of 1 m. Due to the indoor environment, signal reflections and obstructions are significant factors.

The direct link channel $\mathbf{h}_{d,k}$ follows Rayleigh fading and is modelled as $\mathbf{h}_{d,k} \sim \mathbb{CN}(0, I)$. Meanwhile, the channel $\mathbf{O}$ between the BS and IRS, as well as the channels $\mathbf{h}_{r,k}$ between the IRS and the users, follow Rician fading.

$$\mathbf{O} = \beta_1 \left[ \sqrt{\frac{\varepsilon}{1+\varepsilon}} \mathbf{a}_M(\boldsymbol{\phi}_1)\mathbf{a}_N(\boldsymbol{\phi}_2)^{\text{H}} + \sqrt{\frac{1}{1+\varepsilon}} \mathbf{O}_0 \right] \tag{40}$$

$$\mathbf{h}_{r,k} = \beta_{2,k} \left[ \sqrt{\frac{\varepsilon}{1+\varepsilon}} \mathbf{a}_N(\boldsymbol{\phi}_3) + \sqrt{\frac{1}{1+\varepsilon}} \mathbf{h}_{r,k} \right] \tag{41}$$

In this setup, the non-line-of-sight components $\mathbf{O}_0$ and $\mathbf{h}_{r,k}$ follow $\mathbb{CN}(0, I)$. Path losses $\beta_1$ and $\beta_{2,k}$ are considered, with the Rician factor $\varepsilon$ set to 10. The steering vector is $\mathbf{a}$, and angular parameters are $\boldsymbol{\phi}_1, \boldsymbol{\phi}_2$, and $\boldsymbol{\phi}_3$. Path loss for the direct link is $32.6 + 36.7\log(d_1)$, and for the cascaded link, it is $22 + 22\log(d_2)$, where $d_1$ and $d_2$ are the distances between users and the BS. Both uplink and downlink transmission powers are 15 dBm, with noise power at −90 dBm for uplink and −75 dBm for downlink.

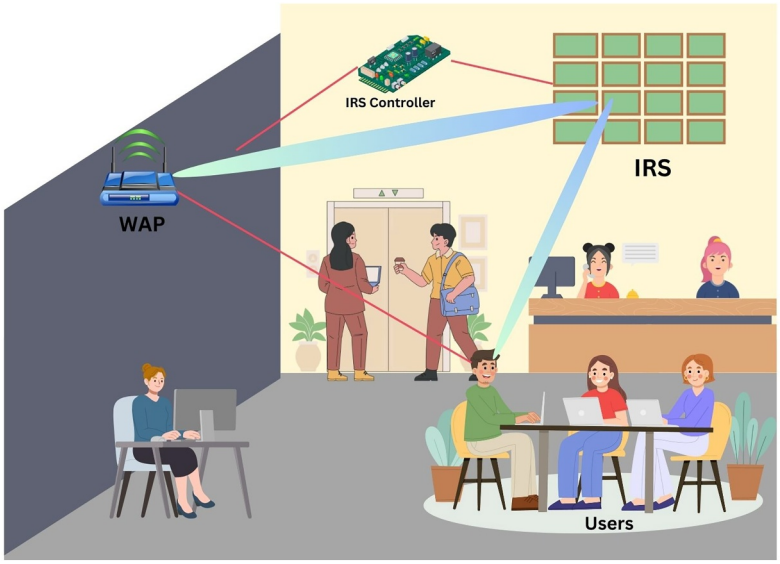


**FIGURE 4** IRS-assisted indoor communication system illustration.

Figure 5 presents an IRS-assisted communication setup, where signals from the BS at coordinates $(15, -15, 2)$ are reflected by the IRS positioned at $(0, 0, 2.5)$ to multiple users located at different positions within the coverage area. User devices are strategically placed at coordinates $(10, 5, 1.5)$, $(20, 5, 1.5)$, and $(15, 10, 1.5)$ to receive optimised signal reflections.

### 4.4.2 | Neural network training

The neural network designed for this study features a 3-layer architecture with dimensions of $150 \times 150 \times 150$, utilising ReLU activation functions in the hidden layers. The implementation is carried out in TensorFlow, and the training process employs the Adam optimiser with an initial learning rate of $10^{-4}$. During each training epoch, the neural network parameters are updated across 50 iterations, and 200 training samples are used to compute gradients in each iteration. During the testing phase, the neural network is evaluated against the perfect CSI with block coordinate descent (BCD) where sum-rate maximisation problem, given perfect CSI, is addressed using the BCD algorithm. The BCD algorithm is halted when the sum-rate increase between consecutive iterations falls below $10^{-3}$. Subsequently, sum-rate maximisation is carried out for the LMMSE estimator are derived from 10,000 channel realisations.

### 4.4.3 | Result analysis

Figure 6 illustrates the sum-rate performance (bps/Hz) of perfect CSI, LMMSE, and GDNNet as the number of users (K) increases. GDNNet consistently outperforms both perfect CSI and LMMSE, showing a steeper increase in sum rate as more users are added. This indicates GDNNet's superior scalability and efficiency in handling multiple users. While all schemes improve with an increasing number of users, GDNNet maintains a significant lead. Specifically, at $K = 8$ users, GDNNet achieves approximately 13 bps/Hz, whereas

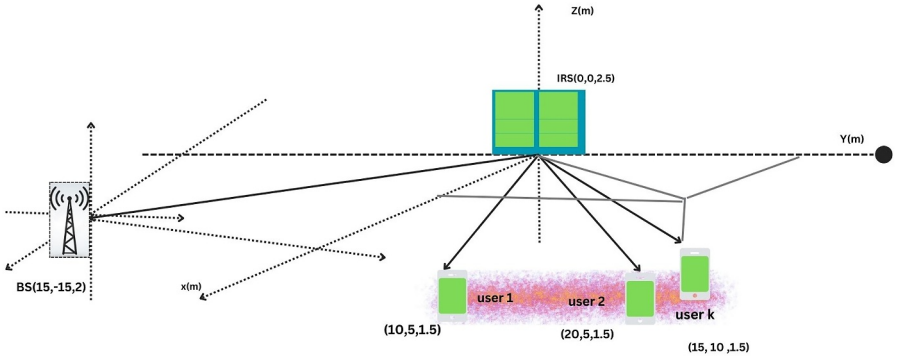


**FIGURE 5** IRS-assisted indoor communication system illustration.

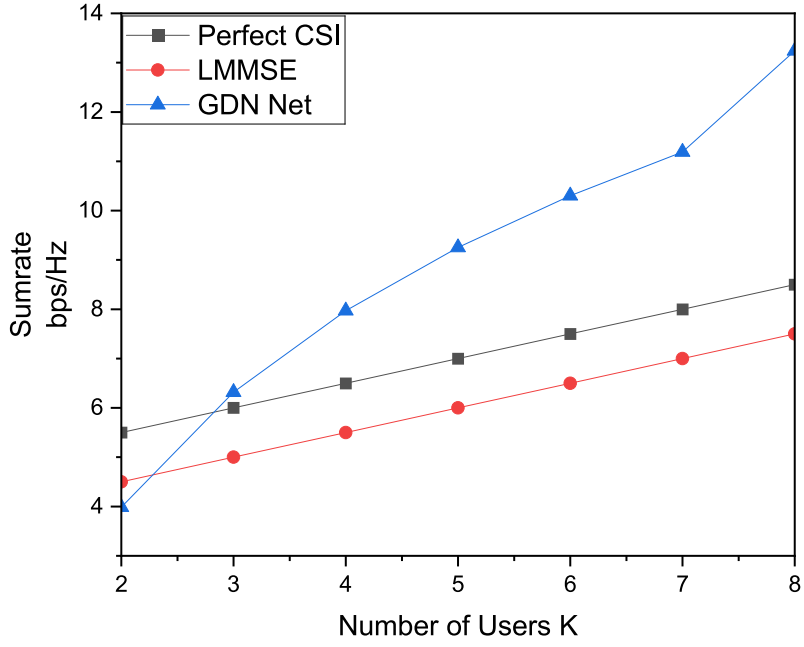


**FIGURE 6** Sumrate versus number of users.

perfect CSI reaches around 9 bps/Hz, and LMMSE only attains about 7 bps/Hz. These numerical values highlight GDNNet's superior performance, making it the most effective scheme for optimising sum rates in multi-user scenarios. Figure 7 compares sum-rate performance (bps/Hz) of perfect CSI, LMMSE, and GDNNet across various transmit power levels. GDNNet consistently demonstrates superior performance over both perfect CSI and LMMSE. At each power level, GDNNet achieves significantly higher sum-rates, showcasing its effectiveness in optimising network utility. This trend is consistent across all measured power levels, highlighting the robustness of the GDNNet approach. In particular, at 25 dBm, GDNNet achieves 18 bps/Hz, while perfect CSI and LMMSE only reach about 7 bps/Hz, clearly indicating the superiority of GDN Net.

Figure 8 compares the sum-rate performance of perfect CSI, LMMSE, and GDNNet across various uplink transmit power levels. GDNNet consistently outperforms both perfect CSI and LMMSE, demonstrating its superior ability to optimise network utility. As the uplink transmit power increases, the gap between GDNNet and the other schemes widens, highlighting its robustness and efficiency. The superior performance of GDNNet is evident at all power levels, indicating its effectiveness in real-world scenarios. Specifically, at 20 dBm,

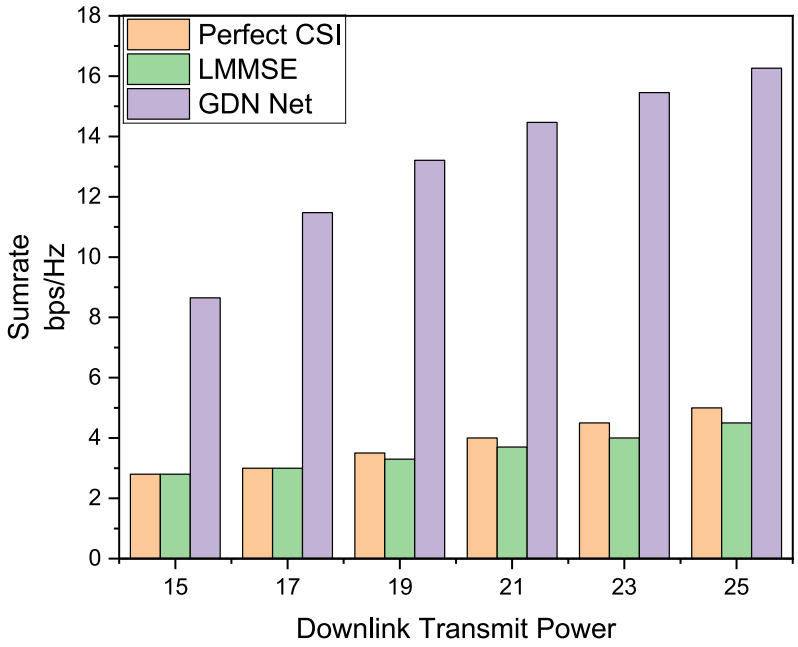


**FIGURE 7** Sum rate versus download transmit power.

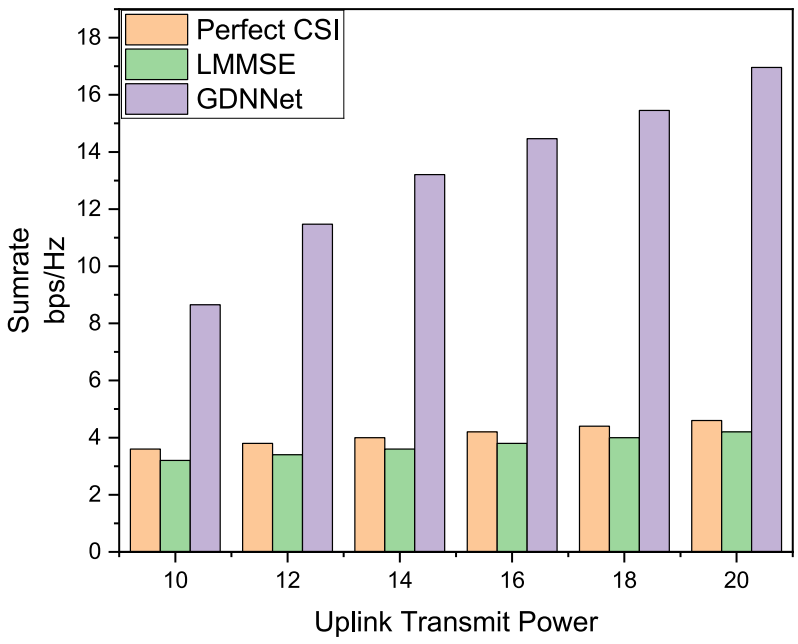


**FIGURE 8** Sum rate versus upload transmit power.

GDNNet achieves a sum-rate of 18 bps/Hz, while perfect CSI and LMMSE only reach about 6 bps/Hz and 4 bps/Hz, respectively, underscoring GDNNet's significant advantage.

Figure 9 shows the sum-rate performance of perfect CSI, LMMSE, and GDNNet as a function of pilot length. GDNNet consistently achieves higher sum rates compared to both LMMSE and perfect CSI across all pilot lengths. As the pilot length increases, all schemes improve, but GDNNet maintains a clear advantage. This demonstrates the efficiency of GDNNet in utilising pilot information for network optimisation. Specifically, at a pilot length of 120, GDNNet reaches a sum rate of 5.5 bps/Hz, while perfect CSI achieves about 5 bps/Hz, and LMMSE only reaches 4 bps/Hz. These numerical values highlight GDNNet's superior performance, making it the most effective scheme for optimising sum rates.

Figure 10 illustrates the empirical CDF of the minimum rate for perfect CSI, LMMSE, and GDNNet. GDNNet consistently shows a higher empirical CDF compared to LMMSE and perfect CSI, indicating better performance across various minimum rates. This trend demonstrates that GDNNet achieves higher rates more reliably than the other

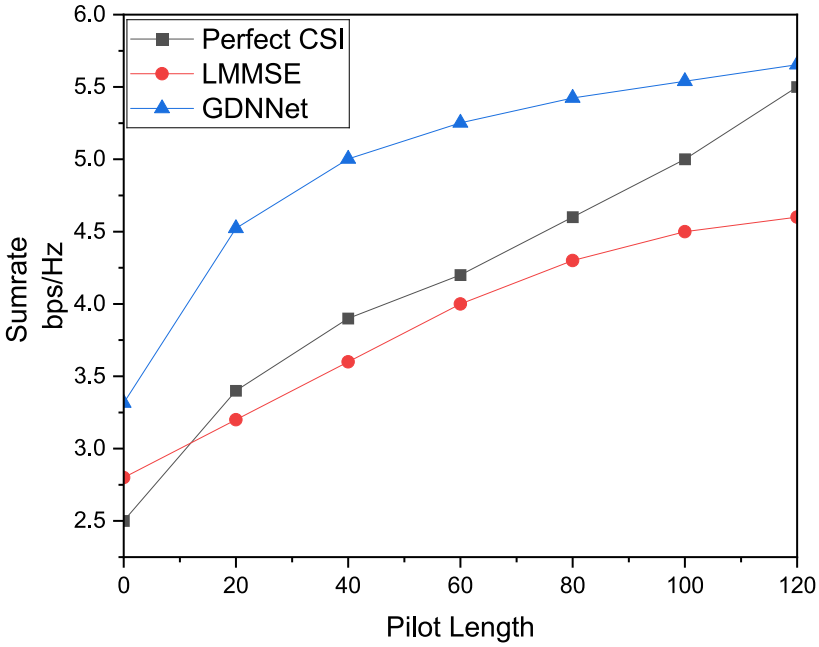


**FIGURE 9** Sumrate versus pilot length.

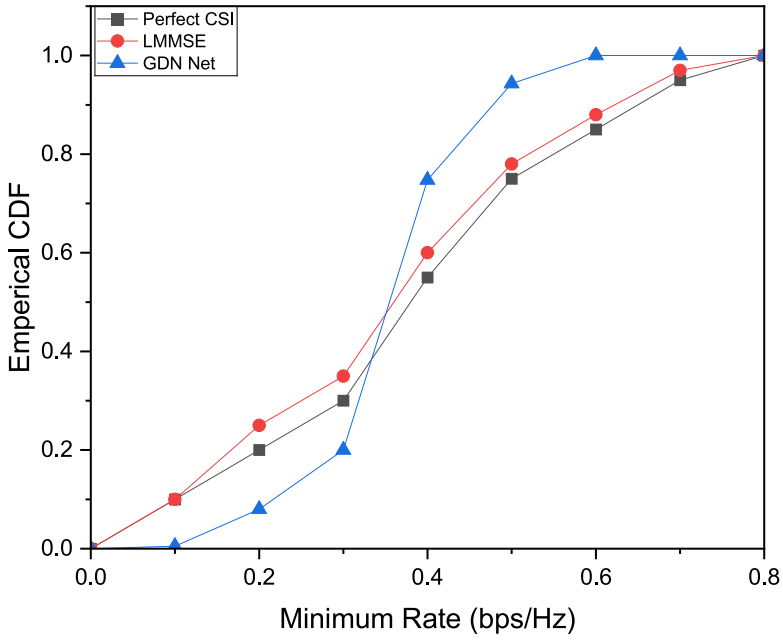


**FIGURE 10** Empirical CDF.

two schemes. As the minimum rate increases, GDNNet maintains a clear advantage, reflecting its robustness in achieving higher performance levels. At a minimum rate of 0.6 bps/Hz, GDNNet reaches an empirical CDF close to 0.9, while LMMSE and perfect CSI lag behind at approximately 0.8 and 0.75, respectively. This numerical evidence highlights the superior capability of GDNNet in providing higher minimum rates, making it the most effective scheme among the three.

## 5 | CONCLUSION

Optimising IRS for multiuser cellular networks presents challenges due to the large number of passive reflective elements, making traditional channel estimation methods impractical. This paper introduces an innovative GNN + DNN framework that directly configures IRS and optimises beamforming at the BS by mapping received pilot signals to system configurations, effectively bypassing explicit channel estimation. Utilising a generalisable GNN architecture, the approach captures user interactions and adapts to varying user numbers. Simulation results demonstrate that the trained neural network efficiently maximises utility functions, such as sum-rate and minimum-rate, using significantly fewer pilots compared to conventional methods. This method outperforms traditional model-based techniques like LMMSE and approaches the performance of perfect CSI, offering a practical and computationally efficient solution for IRS-assisted communication systems. In this, the sum rate for GDNNet shows an improvement of 12.57% over LMMSE and 12.42% over perfect CSI with respect to the number of users, an increase of 28.57% over LMMSE and 14.28% over perfect CSI with respect to pilot length, and a remarkable enhancement of 81% over LMMSE and 75% over perfect CSI with respect to uplink and downlink transmit power.

## AUTHOR CONTRIBUTIONS

**Sakhshra Monga**: Conceptualisation; formal analysis; investigation; methodology; writing - original draft. **Anmol Rattan Singh**: Data curation; funding acquisition; investigation. **Nitin Saluja**: Software; validation. **Chander Prabha**: Methodology; software; writing - review & editing. **Shivani Malhotra**: Methodology; writing - original draft. **Asif Karim**: Conceptualisation; writing - review & editing. **Md. Mehedi Hassan**: Funding acquisition; investigation; project administration; supervision; writing - original draft

## CONFLICT OF INTEREST STATEMENT

To the best of our knowledge, no financial or other conflict of interest exists.

## DATA AVAILABILITY STATEMENT

The dataset is available upon request from the corresponding author.

## ORCID

*Md. Mehedi Hassan* https://orcid.org/0000-0002-9890-0968

## REFERENCES

1. Guo, H., et al.: Weighted sum-rate maximization for reconfigurable intelligent surface aided wireless networks. IEEE Trans. Wireless Commun. 19(5), 3064–3076 (2020). https://doi.org/10.1109/twc.2020.2970061
2. Abeywickrama, S., et al.: Intelligent reflecting surface: practical phase shift model and beamforming optimization. IEEE Trans. Commun. 68(9), 5849–5863 (2020). https://doi.org/10.1109/tcomm.2020.3001125
3. Monga, S., et al.: Learning aided intelligent mechanism for channel estimation in 5g wireless networks. In: 2023 International Conference on Emerging Smart Computing and Informatics (ESCI), pp. 1–6. IEEE (2023)
4. He, Z.-Q., Yuan, X.: Cascaded channel estimation for large intelligent metasurface assisted massive MIMO. IEEE Wireless Commun. Lett. 9(2), 210–214 (2019). https://doi.org/10.1109/lwc.2019.2948632
5. Monga, S., et al.: Optimising multi-user wireless networks through discrete Fourier transform-based channel estimation with cascaded intelligent reflecting surfaces. IET Wirel. Sens. Syst. 14(4), 144–156 (2024). https://doi.org/10.1049/wss2.12081
6. Pan, C., et al.: An overview of signal processing techniques for RIS/IRS-aided wireless systems. IEEE J. Selected Top. Signal Process. 16(5), 883–917 (2022). https://doi.org/10.1109/jstsp.2022.3195671
7. Do, D.-T., Le, A.-T., Mumtaz, S.: Secure performance analysis of RIS-aided wireless communication systems. In: 2021 IEEE Global Communications Conference (GLOBECOM), pp. 01–06. IEEE (2021)
8. Jiang, T., Cheng, H.V., Yu, W.: Learning to reflect and to beamform for intelligent reflecting surface with implicit channel estimation. IEEE J. Sel. Area. Commun. 39(7), 1931–1945 (2021). https://doi.org/10.1109/jsac.2021.3078502
9. Li, H., et al.: Intelligent reflecting surface enhanced wideband MIMO-OFDM communications: from practical model to reflection optimization. IEEE Trans. Commun. 69(7), 4807–4820 (2021). https://doi.org/10.1109/tcomm.2021.3069860
10. Monga, S., et al.: Revolutionizing intelligent reflecting surfaces: deep learning-driven channel estimation. In: 2024 2nd International Conference on Advancement in Computation & Computer Technologies (InCACCT), pp. 148–153. IEEE (2024)
11. Abrardo, A., et al.: MIMO interference channels assisted by reconfigurable intelligent surfaces: mutual coupling aware sum-rate optimization based on a mutual impedance channel model. IEEE Wireless Commun. Lett. 10(12), 2624–2628 (2021). https://doi.org/10.1109/lwc.2021.3109017
12. Rani, S., Ahmed, S.H., Rastogi, R.: Dynamic clustering approach based on wireless sensor networks genetic algorithm for iot applications. Wireless Network 26(4), 2307–2316 (2020). https://doi.org/10.1007/s11276-019-02083-7
13. Sharma, B., Aseri, T.C.: A comparative analysis of reliable and congestion-aware transport layer protocols for wireless sensor networks. Int. Sch. Res. Notices 2012(1), 104057 (2012). https://doi.org/10.5402/2012/104057
14. Alkhateeb, A., et al.: Deep learning coordinated beamforming for highly-mobile millimeter wave systems. IEEE Access 6, 37328–37348 (2018). https://doi.org/10.1109/access.2018.2850226
15. Zhi, K., et al.: Power scaling law analysis and phase shift optimization of ris-aided massive mimo systems with statistical csi. IEEE Trans. Commun. 70(5), 3558–3574 (2022). https://doi.org/10.1109/tcomm.2022.3162580
16. Bai, T., et al.: Resource allocation for intelligent reflecting surface aided wireless powered mobile edge computing in OFDM systems. IEEE Trans. Wireless Commun. 20(8), 5389–5407 (2021). https://doi.org/10.1109/twc.2021.3067709

17. Basar, E., et al.: Wireless communications through reconfigurable intelligent surfaces. IEEE Access 7, 116753–116773 (2019). https://doi.org/10.1109/access.2019.2935192
18. Bottou, L.: Stochastic gradient descent tricks. In: Neural Networks: Tricks of the Trade, ed, pp. 421–436 (2012)
19. Chen, J., et al.: Channel Estimation for Reconfigurable Intelligent Surface Aided Multi-User Mimo Systems (2019). arXiv preprint arXiv: 1912.03619
20. Chen, X., et al.: Low-complexity channel estimation for intelligent reflecting surface-enhanced massive mimo. IEEE Wireless Commun. Lett. 10(5), 996–1000 (2021). https://doi.org/10.1109/lwc.2021.3054004
21. Chen, Y., Wang, Y., Jiao, L.: Robust transmission for reconfigurable intelligent surface aided millimeter wave vehicular communications with statistical CSI. IEEE Trans. Wireless Commun. 21(2), 928–944 (2021). https://doi.org/10.1109/twc.2021.3100492
22. Deng, L., Yu, D.: Deep learning: methods and applications. Foundations Trends® in Signal Processing 7(3–4), 197–387 (2014). https://doi.org/10.1561/2000000039
23. Araújo, G.T., De Almeida, A.L., Boyer, R.: Channel estimation for intelligent reflecting surface assisted mimo systems: a tensor modeling approach. IEEE J. Selected Top. Signal Process. 15(3), 789–802 (2021). https://doi.org/10.1109/jstsp.2021.3061274
24. Chu, Z., et al.: Intelligent reflecting surface aided multi-antenna secure transmission. IEEE Wireless Commun. Lett. 9(1), 108–112 (2019). https://doi.org/10.1109/lwc.2019.2943559
25. Cui, M., Zhang, G., Zhang, R.: Secure wireless communication via intelligent reflecting surface. IEEE Wireless Commun. Lett. 8(5), 1410–1414 (2019). https://doi.org/10.1109/lwc.2019.2919685
26. Di Renzo, M., et al.: Smart radio environments empowered by reconfigurable intelligent surfaces: how it works, state of research, and the road ahead. IEEE J. Sel. Area. Commun. 38(11), 2450–2525 (2020). https://doi.org/10.1109/jsac.2020.3007211
27. Giordani, M., et al.: Toward 6g networks: use cases and technologies. IEEE Commun. Mag. 58(3), 55–61 (2020). https://doi.org/10.1109/mcom.001.1900411
28. Gao, Z., et al.: Compressive sensing techniques for next-generation wireless communications. IEEE Wireless Commun. 25(3), 144–153 (2018). https://doi.org/10.1109/mwc.2017.1700147
29. Gong, S., et al.: Toward smart wireless communications via intelligent reflecting surfaces: a contemporary survey. IEEE Commun. Surv. & Tutorials 22(4), 2283–2314 (2020). https://doi.org/10.1109/comst.2020.3004197
30. Guo, H., Lau, V.K.: Uplink cascaded channel estimation for intelligent reflecting surface assisted multiuser MISO systems. IEEE Trans. Signal Process. 70, 3964–3977 (2022). https://doi.org/10.1109/tsp.2022.3193626
31. He, J., et al.: Learning to estimate RIS-aided mmwave channels. IEEE Wireless Commun. Lett. 11(4), 841–845 (2022). https://doi.org/10.1109/lwc.2022.3147250
32. Kundu, N.K., McKay, M.R.: Channel estimation for reconfigurable intelligent surface aided MISO communications: from LMMSE to deep learning solutions. IEEE Open J. Commun. Soc. 2, 471–487 (2021). https://doi.org/10.1109/ojcoms.2021.3063171

**How to cite this article:** Monga, S., et al.: Advanced beamforming and reflection control in intelligent reflecting surfaces with integrated channel estimation. IET Microw. Antennas Propag. 1–15 (2024). https://doi.org/10.1049/mia2.12538